

## MIT Open Access Articles

*Electrochemistry of Molten Sulfides: Copper  
Extraction from BaS-Cu<sub>2</sub>S*

The MIT Faculty has made this article openly available. **Please share**  
how this access benefits you. Your story matters.

**Citation:** Sokhanvaran, Samira, Sang-Kwon Lee, Guillaume Lambotte, and Antoine Allanore. "Electrochemistry of Molten Sulfides: Copper Extraction from BaS-Cu<sub>2</sub>S." J. Electrochem. Soc. 163, no. 3 (December 31, 2015): D115–D120.

**As Published:** <http://dx.doi.org/10.1149/2.0821603jes>

**Publisher:** Electrochemical Society

**Persistent URL:** <http://hdl.handle.net/1721.1/101746>

**Version:** Final published version: final published article, as it appeared in a journal, conference proceedings, or other formally published context

**Terms of use:** Creative Commons Attribution 4.0 International License





## Electrochemistry of Molten Sulfides: Copper Extraction from BaS-Cu<sub>2</sub>S

Samira Sokhanvaran, Sang-Kwon Lee, Guillaume Lambotte, and Antoine Allanore<sup>\*,z</sup>

Department of Materials Science and Engineering, Massachusetts Institute of Technology, Cambridge, Massachusetts 02139, USA

The electrolytic extraction of liquid copper at 1105°C from a molten sulfide electrolyte composed of 57 wt% BaS and 43 wt% Cu<sub>2</sub>S was investigated. DC cyclic voltammetry, Fourier transformed AC voltammetry, and galvanostatic electrolysis revealed that the electrodeposition of copper is possible in the selected molten sulfide electrolyte. The half wave potential for the reaction on graphite was determined, and liquid copper of high purity was obtained by galvanostatic electrolysis. These preliminary results confirm that molten sulfides free of alkaline elements could be used as an electrolyte for faradaic applications, despite the semi-conducting nature of the melt. In addition to demonstrating the need for enhanced understanding of the transport properties of such electrolyte, the results show the critical impact of the cell design to improve the process faradaic efficiency.

© The Author(s) 2015. Published by ECS. This is an open access article distributed under the terms of the Creative Commons Attribution 4.0 License (CC BY, <http://creativecommons.org/licenses/by/4.0/>), which permits unrestricted reuse of the work in any medium, provided the original work is properly cited. [DOI: 10.1149/2.0821603jes] All rights reserved.

Manuscript submitted October 30, 2015; revised manuscript received December 18, 2015. Published December 31, 2015.

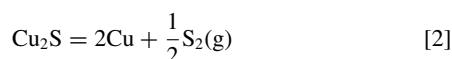
Sulfide-containing ores are the main raw material for copper extraction. The conventional chemical principle underlying metal extraction from such ore (smelting) is the selective oxidation of sulfide ions (S<sup>2-</sup>) by oxygen. The reaction 1 forms copper metal and sulfur dioxide (SO<sub>2</sub>) as products, as written here for chalcocite (Cu<sub>2</sub>S):



Such principle leads to a process characterized by large capital investments and significant environmental challenges.<sup>1</sup> This route requires handling SO<sub>2</sub> as a by-product, typically converted to sulfuric acid. To circumvent this issue, additional pyrometallurgical steps to convert SO<sub>x</sub> into elemental sulfur have been devised, using for example reduction or chlorination.<sup>2</sup>

Hydrometallurgy is an alternative to traditional smelting that does not involve SO<sub>2</sub>.<sup>3-5</sup> It involves a succession of leaching, solvent extraction and finally electrowinning of Cu in an aqueous electrolyte. This route is also characterized by a relatively large footprint and capital cost. One of the limitations is inherited from the electrowinning/refining steps, where the current density for copper electrodeposition is typically limited to 0.05 A.cm<sup>-2</sup>.<sup>6</sup>

An alternative approach to avoid SO<sub>2</sub> formation is the direct decomposition of copper sulfide into copper and elemental sulfur, following reaction 2:



At 1106°C, more than 20°C above copper melting point, reaction 2 is not spontaneous ( $\Delta_r G^\circ = 90.5 \text{ kJ.mol}^{-1}$ ) and would require a minimum amount of energy of 267 kJ.mol<sup>-1</sup> (equivalent to 583 kWh.t<sub>Cu</sub><sup>-1</sup>).<sup>7</sup> This reaction could therefore be driven by electricity, as practiced industrially for most metals, including copper and aluminum. In principle, electrolysis can also offer the selective recovery of multiple metals contained in the sulfides ores, for example elements more noble than copper, e.g. silver or molybdenum.

The direct electrolysis of sulfides was proposed in concept by Townsend in a patent in 1906.<sup>2</sup> Since then, the challenge remains in selecting a supporting electrolyte with an acceptable solubility for copper sulfide concentrates to guarantee large cathode current density, a requirement for tonnage production. Previous studies considered both aqueous solutions and halide melts as possible supporting electrolytes.

Conventional aqueous electrolytes have a limited solubility for the concentrate feedstock, and call for harsh leaching conditions in order

to be effective at liberating copper ions.<sup>3</sup> An alternative approach is the direct electrowinning of the solid sulfides, for example using the sulfide as the anode where the sulfide ions are oxidized to form elemental sulfur while the Cu<sup>+</sup> ions are liberated.<sup>8</sup> Unfortunately, the formation of a non-conductive layer promptly inhibits further reaction at the anode, and hinders further electrolysis.<sup>8</sup> Both approaches have limitations inherited from the production of a solid metal deposit, restricting the productivity of the process.

Therefore, processes operating at a temperature in excess of 1084°C (the melting point of copper) have been envisioned. In such conditions however, the semi-conducting properties of most of the sulfide feedstocks, becomes critical in order to design a satisfactory electrolyte. Electrolysis in molten chloride electrolytes has been demonstrated in 1958, showing remarkable energy efficiency and high current density.<sup>9</sup> Recently, a resurgence in halide-based approach for sulfides electrolysis has been observed for aluminium,<sup>10</sup> tungsten,<sup>11</sup> molybdenum<sup>12</sup> or refining copper.<sup>13</sup> The use of a chloride melt, and CuCl<sub>2</sub> in particular,<sup>14,15</sup> suppresses the electronic conduction of Cu<sub>2</sub>S. However, the low solubility of sulfides in chloride, the sensitivity of such melts to impurities and the limited anodic efficiency due to the competition between sulfur and chlorine evolution from the anode remain key challenges for the molten salt approach.<sup>11-13,16,17</sup>

An alternative strategy is to select molten sulfides as a medium with a high solubility for the sulfide feedstock. Sulfide electrochemical properties have mostly been studied for battery applications, e.g. Li or Na/S batteries.<sup>18,19</sup> Na/S batteries operate at high temperatures (130 to 450°C), with metallic Na as the active material and β-Al<sub>2</sub>O<sub>3</sub> as a separator.<sup>19</sup> The oxidation-reduction processes of sulfur have therefore been investigated in different electrolytes, including sulfide melts, and on different electrodes.<sup>18-22</sup> Voltammetry indicates that the oxidation of sulfide ions (S<sup>2-</sup>) to elemental sulfur is presumably a single step reaction, while sulfur reduction consists in multiple steps<sup>22</sup> leading to the formation of polysulfides of the alkaline metals.<sup>22</sup> The solubility and stability of those species have been reported as the critical challenge for battery applications. Transport properties such as transference number,<sup>23</sup> diffusion coefficient<sup>24</sup> or conductivity<sup>25</sup> of sodium polysulfides have therefore been studied, revealing that Na<sup>+</sup> cations are the major charge carrier.<sup>23</sup>

The electrochemical properties of molten sulfides (Na<sub>2</sub>S-NiS and Na<sub>2</sub>S-FeS) at high temperature have been investigated using voltammetry, in the context of the corrosion of Ni-based alloys in fossil fuels reactors.<sup>26</sup> This study concludes the possibility of a sulfide/polysulfide reaction at the anode based on polarization data and a qualitative evaluation of the possible electron-exchange reactions. There is altogether a need to confirm the suitability of molten sulfides to conduct faradaic reactions, particularly in the context of metal extraction or deposition.

\*Electrochemical Society Active Member.

<sup>z</sup>E-mail: [allanore@mit.edu](mailto:allanore@mit.edu)

<sup>a</sup>This energy is calculated considering the feed material is charged at 25°C and the reaction is conducted at 1106°C.

Indeed, most sulfide compounds exhibit metallic or semi-conducting behavior in their solid and liquid phases,<sup>27</sup> properties which are incompatible with the definition of an electrolyte. For example, molten FeS is reported<sup>28</sup> to be a metallic conductor (conductivity of  $1500 \text{ ohm}^{-1}\cdot\text{cm}^{-1}$ ) while molten  $\text{Cu}_2\text{S}$  is a semiconductor.<sup>29,30</sup> Previous work on the electrolytic decomposition of molten sulfides (mattes) for metal extraction by metallurgists is incomplete and lacks consensus, with some referring to the presence of metallic bonding,<sup>27</sup> with others predicting that  $\text{Cu}_2\text{S}$  dissociates to  $\text{Cu}^+$  and  $\text{S}^{2-}$  in the melt with  $\text{S}^{2-}$  ions engaging in weak covalent bonds.<sup>14</sup> This last work reports the impossibility of decomposing pure molten  $\text{Cu}_2\text{S}$ , as anticipated from its solid-state bandgap (1.21 eV<sup>31</sup>) and electronic conductivity in the molten state ( $70 \text{ ohm}^{-1}\cdot\text{cm}^{-1}$ ).<sup>29,30</sup>

Clearly, a suitable electrolyte for metal extraction must limit the large electronic conduction inherent in the feed materials. This can be accomplished by adding a species with ionic bonding characteristics. Among sulfides, alkali and alkali earth metals exhibit the largest electronegativity difference vs. sulfur, and presumably exhibit such ionic bonding, as reported for a limited number of metal sulfides/alkali sulfides.<sup>17</sup> Several measurements of the total electrical conductivity of molten sulfides containing  $\text{Na}_2\text{S}$  or  $\text{K}_2\text{S}$  mention a relative suppression of the nonionic behavior of metallic sulfides (i.e. Sb, Sn, Tl,<sup>32,33</sup> Ag<sup>34</sup>), a conclusion drawn from the drastic increase in the melt resistivity observed upon addition of the alkali sulfide. In the spirit of that reasoning, a single study dedicated to copper extraction by electrolysis from a sulfide is available in the open literature, proposing to operate with a binary  $\text{Cu}_2\text{S}$ - $\text{Na}_2\text{S}$ .<sup>35</sup> Though not reporting any copper production, this work indicated that the addition of  $\text{Na}_2\text{S}$  lowers the share of electronic conduction of molten  $\text{Cu}_2\text{S}$ .

Our study reports the first effectual electrolytic production of liquid copper from copper (I) sulfide ( $\text{Cu}_2\text{S}$ ) in a binary sulfide electrolyte, using BaS as the additional electrolyte constituent.

The solid-state properties of BaS are indicative of a partial ionic nature: it exhibits a relatively large electronegativity difference on the Pauling scale (1.69 vs. 2.23 for NaCl), a large bandgap<sup>37</sup> (3.92 eV<sup>36</sup> vs. 1.21 eV for  $\text{Cu}_2\text{S}$ <sup>31</sup>), and a small electrical conductivity ( $0.01 \text{ ohm}^{-1}\cdot\text{cm}^{-1}$  vs.  $70 \text{ ohm}^{-1}\cdot\text{cm}^{-1}$  for  $\text{Cu}_2\text{S}$ ). Consequently, the electrical behavior of the binary BaS- $\text{Cu}_2\text{S}$  is anticipated to exhibit a non-negligible share of ionic conduction depending on the composition and the temperature. Independent of such static condensed matter considerations, which ignore the role of transport phenomena and faradaic reactions, the question of the electrolytic performance of such a melt for metal extraction, particularly in terms of cathode faradaic efficiency, remains open.

Herein, we report findings related to the direct electrolysis of one composition in the binary BaS- $\text{Cu}_2\text{S}$  at  $1105^\circ\text{C}$ . This study provides a first insight into the underlying cathodic electrochemical reactions via DC and AC voltammetry. The results of galvanostatic experiments are also reported, confirming the extraction of liquid copper from a molten sulfide melt.

## Experimental

**Electrolyte Preparation.**—The working temperature for the electrochemical measurements was selected to be more than  $20^\circ\text{C}$  above the melting point of copper, at  $1105^\circ\text{C}$ , to ensure liquid metal production. The electrolyte composition was chosen from the reported BaS- $\text{Cu}_2\text{S}$  phase diagram<sup>38</sup> reproduced in Figure 1, in which a homogeneous liquid is expected to form at 44.7 mol%  $\text{Cu}_2\text{S}$  (43.2 wt%) and 55.3 mol % BaS (56.8 wt%). The liquidus drawn in the BaS-rich side of the diagram (dash line) is a graphical extrapolation to the reported melting point of BaS, since there are no experimental data available.

Barium and copper (I) sulfides (BaS, 99.7%,  $\text{Cu}_2\text{S}$ , 99.5% metals basis, Alfa Aesar) powders were mixed in a polystyrene dish, starting with the former (55.3 mol % BaS and 44.7 mol %  $\text{Cu}_2\text{S}$ ). The powders were mixed with a stainless steel spatula, and the mixture was transferred to a graphite crucible (less than 50 ppm ash content) of 14.5 mm inner diameter and 25.4 mm depth. The crucible was placed in a fused quartz tube (Technical Glass Products,

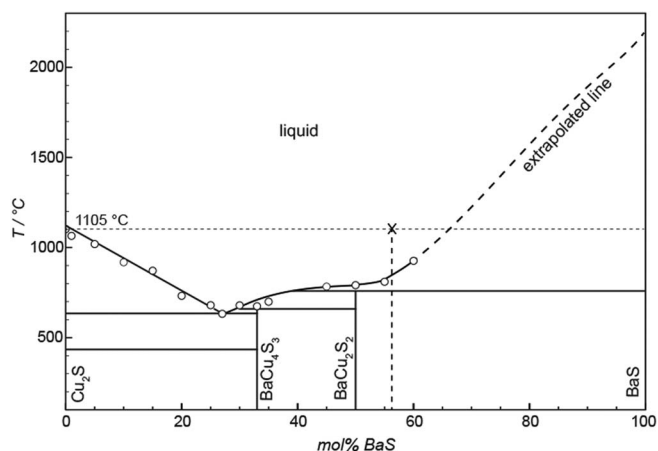


**Figure 1.** Simplified phase diagram for the  $\text{Cu}_2\text{S}$ -BaS system.<sup>38</sup> The circles corresponds to the reported transition points, the dashed line indicates the operating temperature selected in the present work and the cross represents the electrolyte composition.

Inc.) and heated under argon (99.999% purity min.) atmosphere with a tube furnace (Lindberg/Blue 26 M Mini-Mite). The furnace temperature was maintained at  $200^\circ\text{C}$  for 1 hour with argon flow at  $20 \text{ mL}\cdot\text{min}^{-1}$  to remove moisture. The temperature was then increased at  $17.5^\circ\text{C}\cdot\text{min}^{-1}$  to the set point of  $1105^\circ\text{C}$ , with a minimal flow of argon ( $<1 \text{ mL}\cdot\text{min}^{-1}$ ). This temperature was held for 3 hours. After furnace shutdown, the time-averaged cooling rate was  $18^\circ\text{C}\cdot\text{min}^{-1}$  under argon flow at  $40 \text{ mL}\cdot\text{min}^{-1}$  until a temperature of around  $600^\circ\text{C}$ . The weight loss during this procedure was less than 2%.

**Electrodes for electrochemical measurements.**—Graphite rods of 38.1 mm length (99.9995% purity, Alfa Aesar) and of 3.05 mm and 1.76 mm diameter were used as counter and pseudo-reference electrodes, respectively. The working electrode was a graphite rod of 2.4 mm diameter embedded in an alumina tube of 4 mm outer diameter, which served as a sheath. The corresponding exposed geometrical area was then  $0.045 \text{ cm}^2$ . Molybdenum wires were used as current lead to the graphite electrodes. Different electrode configurations were used for different measurements. For the electrochemical measurements (DC & AC voltammetry), the electrodes were moveable in the z-direction and configured in triangle at the top of the crucible, immersed at the top of the electrolyte. For galvanostatic measurements, the working and reference electrodes were fixed and located at the bottom of the crucible, and the anode was tubular (OD 6.57 mm, ID 4.85 mm and 50 mm length). In order to control the current path between the anode and the cathode, the outer surface of the former was protected with an alumina tube (98 wt% purity). The electrical connection to the anode was a threaded stainless steel tube. The corresponding anode area is  $0.92 \text{ cm}^2$  assuming the inner tube walls are electrochemically active (immersion 5 mm). More realistically, and according to the primary current distribution, only the horizontal ring facing the cathode is electrochemically active, leading to an area of  $0.15 \text{ cm}^2$ . This configuration (see Figure 2), despite leading to an anode current density around 10 times smaller than the cathode, proved to facilitate the escape of the gas from the anode surface.

**Process operation.**—The electrodes and the graphite crucible containing the electrolyte were placed in a quartz tube purged with argon at  $20 \text{ mL}\cdot\text{min}^{-1}$ . The heating procedure described in the Electrolyte preparation section was also followed in this step, and the temperature was held for 1 hour at  $1105^\circ\text{C}$  before inserting the moveable electrodes into the melt and conducting electrochemical measurements.

The electrodes were immersed into the bath until electrical contact was achieved. The immersion depth of the anode was 5 mm. Conducting this procedure without applying electrochemical signals did not cause the formation of metallic copper, pointing to the thermodynamic

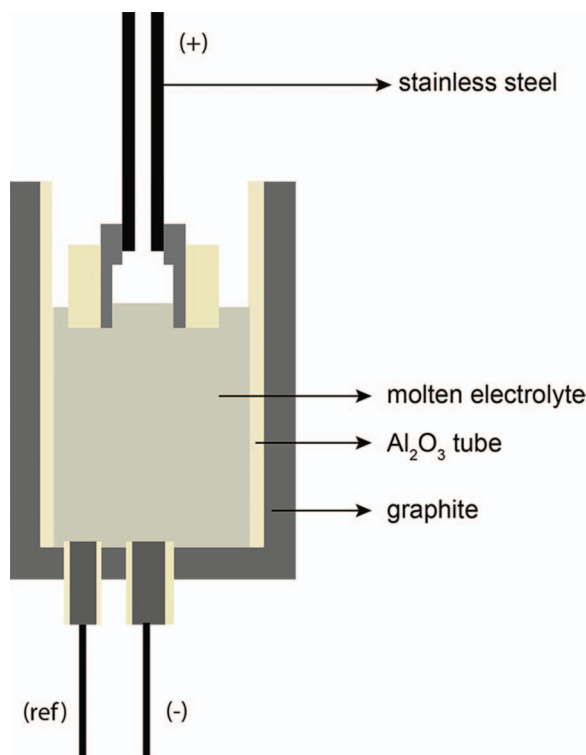


**Figure 2.** Schematic of the cell configuration used for the electrolysis experiments.

stability of copper sulfide in the selected melt in presence of the electrode/crucible assembly under the operating conditions.

**Electrochemical measurements.**—Open circuit potential (OCP), direct-current (DC) cyclic voltammetry, impedance spectroscopy at OCP, and galvanostatic electrolysis measurements were all conducted with the same potentiostat/galvanostat (Reference 3000, Gamry). For alternating-current (AC) voltammetry measurements, a sine wave of fixed amplitude and frequency generated by a 24 bit digital-to-analog audio interface (UltraLite-mk3 Hybrid, Motu) was superimposed onto the DC potential ramp. Analog potential and current responses were collected at the outlets of the potentiostat at a sampling rate of 20,000 samples per second using an analog-to-digital data acquisition system (DT9837, Data Translation). All signal processing, such as Fourier and inverse Fourier transform, was performed using a LabView code. Potentials in this work are referred to the graphite pseudo-reference and corrected post-measurements by 60% of the ohmic resistance measured between the working and reference electrodes at OCP using impedance spectroscopy. The anode, cathode and cell potential during the galvanostatic measurements were recorded using an Omega data acquisition system (OMB-DAQ-54).

**Observation and analysis.**—Samples were stored in a controlled atmosphere storage cabinet before further analysis and characterization. After the experiment, the ensemble composed of the crucible, the electrodes and the electrolyte was mounted in epoxy resin (EpoKwick, Buehler) and cured in air for 24 hours. After cleaving using a hacksaw, the sample was ground with silicon carbide papers (grit up to 1200) using Kerosene as a lubricant, and polished up to 1  $\mu\text{m}$  using a diamond solution. Observations were conducted with optical (Olympus BX51, Olympus) and scanning electron microscopes (JEOL JSM-6610LV, JEOL Ltd.). The SEM was equipped with energy dispersive spectroscopy (EDS, Sirius SD detector, SGX Sensortech Ltd.) for elemental analysis. Compositions were occasionally confirmed with wavelength dispersive spectroscopy (JEOL JXA-8200 Superprobe). Faradaic efficiency estimates are calculated from the weight of copper recovered. The copper droplets were collected from the electrolyte af-

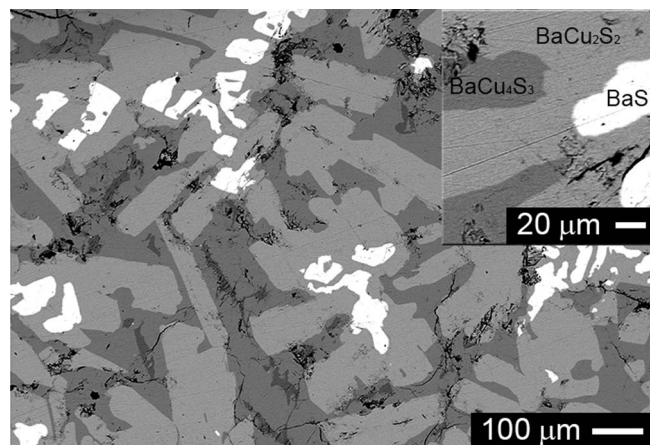


**Figure 3.** Back-scattered electron image of a cross-section of the solidified electrolyte after preparation.

ter electrolysis. The attached electrolyte was removed using a stainless steel tweezer. The weight of the deposited copper was measured using a scale (Sartorius, 0.001 g accuracy), and compared with the prediction from Faraday's law, assuming a one-electron transfer process.

## Results

**Electrolyte microstructure.**—Figure 3 is a back-scattered electrons (BSE) image of the solidified electrolyte after its preparation, obtained following the procedure described above. Three solidified phases are distinguishable, labeled BaS, BaCu<sub>2</sub>S<sub>2</sub>, and BaCu<sub>4</sub>S<sub>3</sub> according to the phase diagram and the results of wavelength dispersive X-ray spectroscopy (WDS). The microstructure follows qualitatively what is expected from the phase-diagram and a quasi-equilibrium solidification: a minute amount of BaS solidifies first. This event leads to the rejection of Cu<sub>2</sub>S, leading to the formation of Cu<sub>2</sub>S-rich compounds of lower melting point, in an amount which increases with their decreasing BaS content.

**Voltammetry measurements.**—The feasibility of conducting faradaic reactions in this melt was investigated using both direct (DC) and alternating current (AC) electrochemical techniques. Figure 4

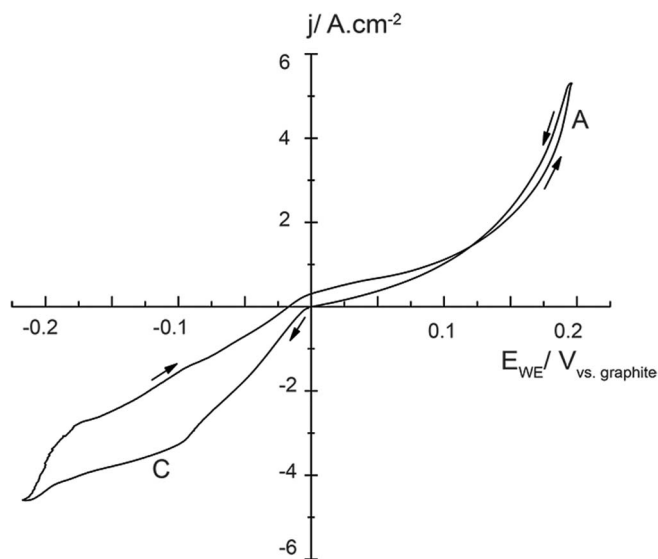


**Figure 4.** First cycle of a cyclic voltammogram in molten BaS-Cu<sub>2</sub>S at a scan rate of 5  $\text{mV}\cdot\text{s}^{-1}$  at 1105°C, starting polarization in the negative direction from the open circuit potential ( $\sim -0.3$  mV vs. graphite). The labels C and A represent the cathodic current plateau and the anodic wall, respectively.



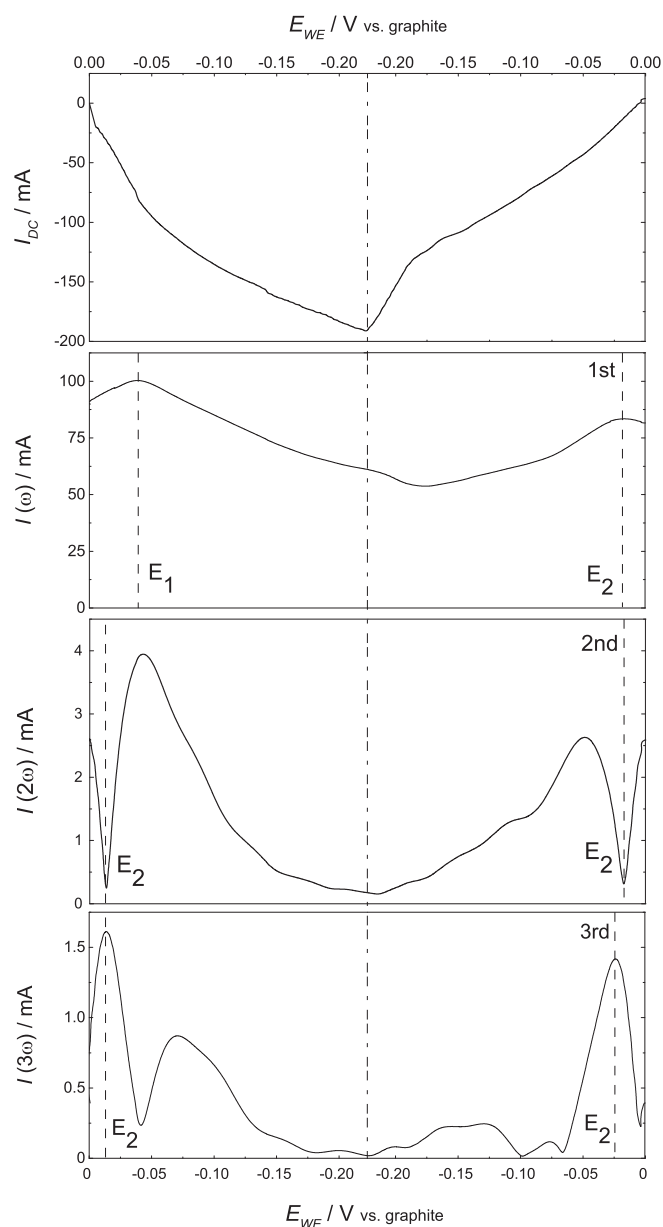


**Figure 5.** DC, fundamental, second, and third harmonic currents measured during AC cyclic voltammetry at a scan rate of  $5 \text{ mV}\cdot\text{s}^{-1}$  at  $1105^\circ\text{C}$ , with a sine wave amplitude and frequency at  $80 \text{ mV}$  and  $10 \text{ Hz}$ , respectively.  $E_1$  and  $E_2$  represent the potential at peak current in the fundamental harmonic and the half wave potential in the  $2^{\text{nd}}$   $\sim$   $3^{\text{rd}}$  harmonics, respectively. Band selection is  $0 \sim 1 \text{ Hz}$  for the DC component,  $10 \pm 1 \text{ Hz}$ ,  $20 \pm 0.1 \text{ Hz}$ , and  $30 \pm 0.09 \text{ Hz}$ , for the  $1^{\text{st}}$   $\sim$   $3^{\text{rd}}$  harmonics, respectively.

shows a DC cyclic voltammogram recorded on the graphite working electrode, where a current plateau at  $4 \text{ A}\cdot\text{cm}^{-2}$  (label C) is observed until around  $-0.185 \text{ V}/\text{ref}$ , after which the current further decreases. The anodic portion of the sweep exhibits a monotonic current increase, with steep increase at around  $0.19 \text{ V}/\text{ref}$ . Measurements at a scan-rate higher than  $5 \text{ mV}\cdot\text{s}^{-1}$  did not reveal any distinctive features in this electrolyte and cell configuration. Fourier transformed (FT) AC voltammetry was conducted to isolate the relative contribution of faradaic and non-faradaic currents (e.g. double layer or adsorption phenomena<sup>39–43</sup>) using second and higher harmonics. DC and AC components are distinguishable from the power spectrum, and the appropriate band selection for the inverse Fourier transformation provides their respective components in the time domain, presented in Figure 5. The DC component reproduces the DC voltammogram of

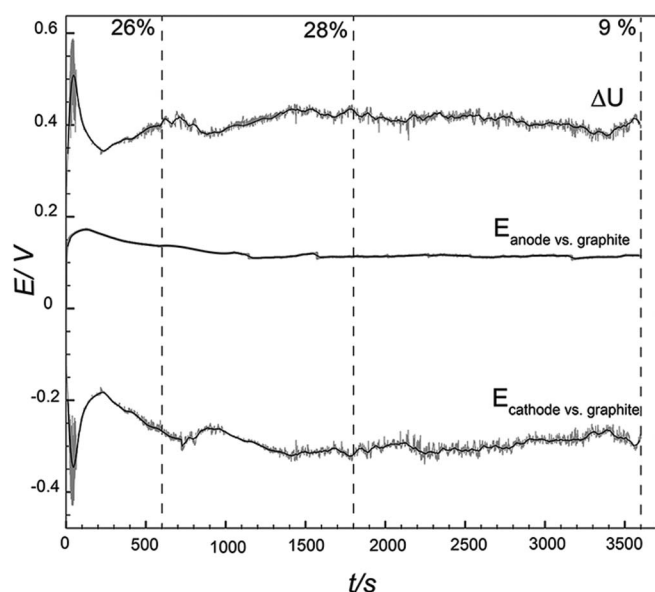


**Figure 6.** Variation of the anode and cathode potentials and cell voltage ( $\Delta U$ ) during galvanostatic electrolysis at a cathode current density of  $2.5 \text{ A}\cdot\text{cm}^{-2}$  during 1 hour. The plain lines are drawn to guide the eyes, and the gray lines present the raw data. Dashed line represent different electrolysis period (data not shown), and the numbers in percent the estimated current efficiency.

Figure 4, confirming that the AC perturbation did not affect the DC phenomena.  $2^{\text{nd}}$  and higher harmonics confirm the occurrence of a faradaic reaction with a half-wave potential ( $E_2$ ) between  $-0.014$  and  $-0.019 \text{ V}/\text{ref}$ . The  $1^{\text{st}}$  harmonic measured during the forward scan exhibits a peak potential ( $E_1$ ) more anodic than  $E_2$ . This anodic offset of  $E_1$  is not observed in the subsequent scans.

**Galvanostatic measurements.**—Galvanostatic electrolysis experiments have been performed to verify the production of liquid copper in accordance with reaction 2. Preliminary experiments showed a large variability in the measured faradaic efficiency, often limited to 5%, which was attributed to the back reaction between the anodic ( $\text{S}_2$ ) and cathodic ( $\text{Cu}$ ) products as well as difficulty in recovering a single copper droplet. These issues have been partly addressed by a careful redesign of the electrochemical cell. One such improved cell design is presented in Figure 2 in which the tubular shape of the anode provides an escape path for the evolving gas. Figure 6 shows the typical variation of both the electrode potentials and the cell voltage with time during galvanostatic electrolysis at a cathode current density of  $2.5 \text{ A}\cdot\text{cm}^{-2}$ . The corresponding anode density is around  $0.25 \text{ A}\cdot\text{cm}^{-2}$ . The measured cell voltage matches the thermodynamic prediction using the Nernst equation for reaction 2, with a minimum cell voltage of  $0.480 \text{ V}$  at  $1105^\circ\text{C}$  and a partial pressure of  $\text{S}_2$  at  $2.0 \times 10^{-7} \text{ atm}$ .<sup>7</sup> The variation of the cell voltage during electrolysis follows those of the cathode potential, while the anode potential is relatively constant.

The optical micrographs of the cell, cathode and anode areas as well as a scanning electron microscope (SEM) images of a droplet recovered after electrolysis are presented in Figures 7 and 8. Lustrous, metal-like, orange-colored droplets are found next to the graphite cathode (Fig. 7a). Imaging (Figures 7b and 7c) combined with electron dispersive spectroscopy (EDS) analysis of cross-sections show that the droplet is indeed metallic, with an average copper content of the metal phase greater than 98 wt%. The gray-colored inclusions (Figure 7c) appear to be  $\text{Cu}_2\text{S}$  particles from EDS analysis. Evidences of a gas phase near the anode in the solidified electrolyte are visible in the optical micrograph in the form voids near the anode or entrapped in the electrolyte (Figure 7b). SEM observations and EDS analysis of the electrolyte surrounding the cathode (Figure 8a) shows a depletion in  $\text{Cu}_2\text{S}$  (resp. an enrichment in  $\text{BaS}$ ), contrary to the bulk electrolyte in which microstructure and average composition are unchanged

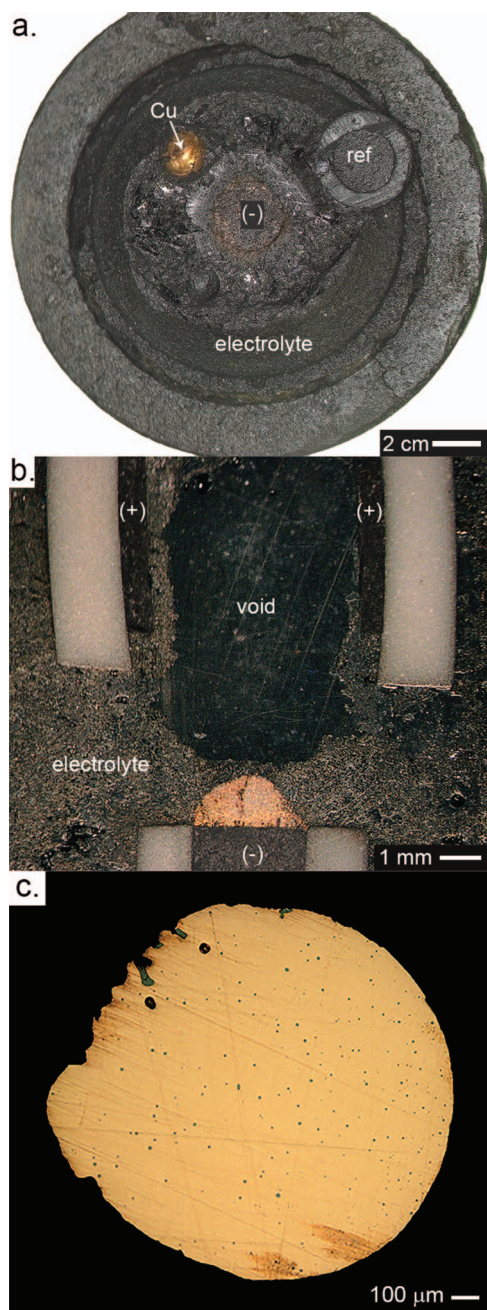


**Figure 7.** a) Optical micrograph of the crucible, view from the bottom after removal of the crucible, b) Optical image of a cross-section of the cell illustrating the formation of a void due to gas evolution (10 min. run), c) Optical image of a droplet of copper recovered in the electrolyte, in cross-section (same run as 7a). EDS analysis show that the metal phase is more than 98 wt%Cu and that the inclusions consist in  $\text{Cu}_2\text{S}$ .

during electrolysis (see Figures 3 and 8b, respectively before and after electrolysis).

Faradaic efficiency measurements for increasing electrolysis duration are also reported in Figure 6. There is a non negligible uncertainty in those measurements due to the difficulty in recovering of all the metallic droplets which often leave the graphite cathode because of surface tension effects. The results suggest a fair efficiency for copper production in the early stages of electrolysis, with up to 28% faradaic efficiency. At longer electrolysis times a decrease in the faradaic efficiency is observed (dashed line and numbers in percent in Figure 6).

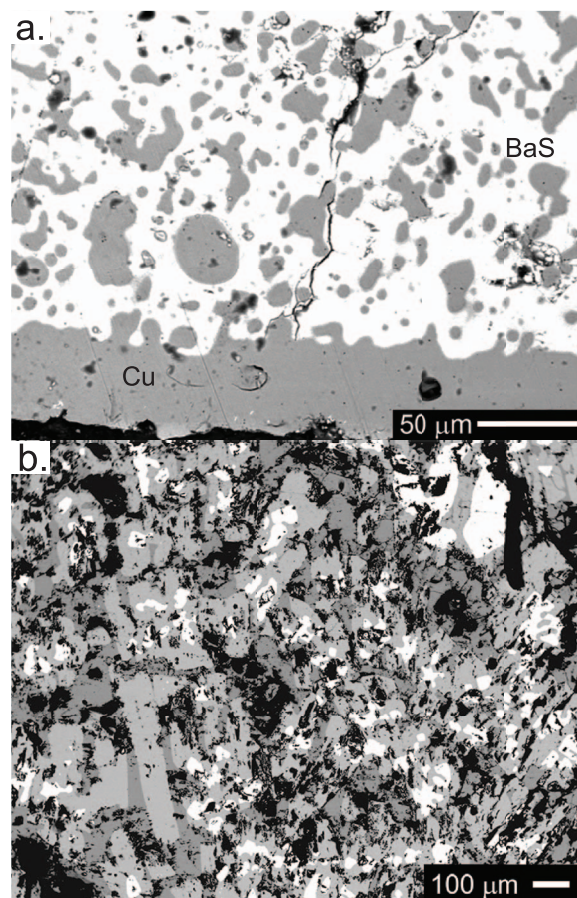


**Figure 8.** a) BSE image of the electrolyte near the cathode after electrolysis (30 min run), in cross-section, b) BSE image of the bulk electrolyte after electrolysis (same run as 8a).

## Discussion

The results of both dynamic (DC and AC voltammetry) and static (constant current) measurements indicate that the electrolysis of the selected  $\text{BaS-Cu}_2\text{S}$  electrolyte enables the formation of metallic copper on the cathode at a cell voltage in reasonable agreement with the thermodynamic predictions for reaction 2. The selective decomposition of copper is in agreement with the decomposition potential series, which predicts that  $\text{BaS}$  is more stable than  $\text{Cu}_2\text{S}$ . The cathode current density is very high (up to  $4 \text{ A}\cdot\text{cm}^{-2}$  assuming the plateau C in Figure 4 is indeed controlled by mass-transfer), as anticipated from the relatively high concentration of cations in the electrolyte. According to the faradaic efficiency estimated in this work, about one third of that current at  $2.5 \text{ A}\cdot\text{cm}^{-2}$  leads to recoverable copper in the proposed cell configuration.

Mass transport during electrolysis plays a key role, in particular leading to the formation of  $\text{BaS}$  in-situ near the cathode due to depletion in Cu (see Figure 8a), an inhomogeneity that will locally affect the electrical and other transport properties. The decrease of the measured faradaic efficiency with time (Figure 6) may be rationalized by the development of a copper-content gradient, though no definite trend in the variation of the depletion layer thickness with time of electrolysis has been observed in these experiments.

The simultaneous formation of a gas phase is observed, over a potential range in agreement with predictions for the evolution of elemental sulfur. The wall-like nature of signal A observed in DC cyclic voltammogram (Figure 4) is an additional result that suggests the decomposition of the electrolyte. Yet, the exact nature of the anodic reaction remains to be confirmed. The direct anodic production of  $\text{CS}_2$  is considered unlikely according to prior results of sulfur evolution



with a graphite anode.<sup>12</sup> No evidences of crystalline polysulfides have been found by XRD measurements (data not shown), though the presence of amorphous material has been noticed particularly at angles that typically correspond to polymeric sulfur.

The estimated faradaic efficiency proves very dependent on the electrolysis cell configuration and the ability to measure and completely recover the anode and cathode products. In particular, the metal product recovery is often hindered by the dispersion of the metallic droplets due to surface tension effects (see the formation of droplets in Figures 7a and 8a), which are particularly important at such small scale.

Concerning the nature of the electrochemical reactions, the present work reports the ability to perform AC voltammetry in such an electrolyte, with cathodic signals that qualitatively match those observed in other electrolytes for metal deposition (see Figure 5 and a recent reference<sup>44</sup> which reports AC voltamogram during copper aqueous electrodeposition). Further progress in modeling the AC signal for metal deposition will enable delineation between faradaic and non-faradaic contributions to the electrochemical signals.

Our results therefore provides evidences that faradaic reactions can be conducted in a molten BaS-Cu<sub>2</sub>S electrolyte, with a minimum of 28% of the supplied charge during electrolysis being transported by ions. This partial ionicity leads to the electrolytic production of copper on the cathode and enables the use of AC-voltametry techniques.

### Conclusions

The ability to extract liquid copper from molten BaS-Cu<sub>2</sub>S melt at 1105°C has been demonstrated. DC and AC voltammetry revealed that faradaic reactions can be conducted, indicating the partial ionic nature of the selected sulfide melt. The production of copper has been confirmed by galvanostatic electrolysis and high purity copper (>98 wt%) has been obtained. Longer time and dedicated set-up are requested to study the corresponding anodic reaction and its efficiency. The present results indicate that molten sulfides can be considered as a possible supporting electrolyte for metal extraction application. The results also highlight the need for dedicated studies of the electrolyte properties, the electrolysis cell design, and the electrochemical response. In particular, it is foreseen that quantifying the relation between electronic conductivity and faradaic efficiency across the BaS-Cu<sub>2</sub>S binary melt is necessary to optimize the electrolyte composition and cell design.

### Acknowledgments

The authors acknowledge Norco Conservation and the Office of Naval Research (contract N00014-12-1-0521) for their financial support to this project.

### References

1. M. E. Schlesinger, M. J. King, K. C. Sole, and W. G. Davenport, *Extractive Metallurgy of Copper*, 5th ed., Elsevier Science, New York (2011).
2. F. Habashi, *The Recovery of Elemental Sulfur from Sulfide Ores*, Butte, Montana College of Mineral Science and Technology (1966).
3. C. Paynter, *J. South African Inst. Min. Metall.*, 158 (1973).
4. J. C. Wilmot, R. Smith, and R. Brewer, in *34th Annual Hydrometallurgy Meeting*, p. 77, Metsoc, Bannf (2004).
5. F. Habashi, *J. Min. Metall. Sect. B Metall.*, 43, 1 (2007).
6. D. Creber, G. Holywell, M. Free, M. Moats, T. Robinson, N. Neelameggham, G. Houlachi, and M. Ginatta, in *Electrometallurgy 2012*, M. Free, M. Moats, G. Houlachi, E. Asselin, A. Allanore, J. Yurko, and S. Wang, Editors, p. 3, Wiley (2012).
7. C. W. Bale et al., *Calphad*, 33, 295 (2009).
8. S. Venkatchalam, *Miner. Eng.*, 4, 1115 (1991).
9. R. G. Hoar and T. P. Ward, *Inst. Min. Metall.*, 618, 393 (1958).
10. D. W. Van Der Plas, 21 U.S. Pat. No. 2004088000 (2004).
11. T. Wang et al., *Electrochem. Commun.*, 13, 1492 (2011).
12. G. Li, D. Wang, X. Jin, and G. Z. Chen, *Electrochem. Commun.*, 9, 1951 (2007).
13. G. Z. Chen and D. J. Fray, *J. Appl. Electrochem.*, 31, 155 (2001).
14. L. Yang, G. M. Pound, and G. Derge, *J. Met.*, 8, 783 (1956).
15. A. Garbee, *J. Electrochem. Soc.*, 119, 631 (1972).
16. X. Ge, X. Wang, and S. Seetharaman, *Electrochim. Acta*, 54, 4397 (2009).
17. N. Quang-Minh and N.-P. Yao, in *Advances in molten salt chemistry*, G. Mamantov, Editor, vol. 5, p. 231, Elsevier, New York (1983).
18. P. G. Bruce, S. A. Freunberger, L. J. Hardwick, and J.-M. Tarascon, *Nat. Mater.*, 11, 172 (2011).
19. P. G. Bruce, L. J. Hardwick, and K. M. Abraham, *MRS Bull.*, 36, 506 (2011).
20. H. Yamin, J. Penciner, A. Gorenshain, M. Elam, and E. Peled, *J. Power Sources*, 14, 129 (1985).
21. G. Babu, K. Ababtain, K. Y. S. Ng, and L. M. R. Arava, *Sci. Rep.*, 5, 8763 (2015).
22. X. Ji and L. F. Nazar, *J. Mater. Chem.*, 20, 9821 (2010).
23. T. Risch, *J. Electrochem. Soc.*, 135, 1715 (1988).
24. S. D. Thompson, *J. Electrochem. Soc.*, 136, 3362 (1989).
25. M.-H. Wang, *J. Electrochem. Soc.*, 142, 761 (1995).
26. C. T. Liu and O. F. Devereux, *J. Electrochem. Soc.*, 131, 247 (1984).
27. G. M. Pound, G. Derge, and G. Osuch, *J. Met.*, 7, 481 (1955).
28. W. Savelsberg, *Ztschr. Elektrochem.*, 46, 379 (1940).
29. E. A. Dancy and G. J. Derge, *Trans. Metall. Soc. AIME*, 227, 1033 (1963).
30. J. E. Enderby and A. C. Barnes, *J. Electroanal. Chem.*, 134, 2483 (1987).
31. Y. Wu et al., *Am. Chem. Soc.*, 8, 2551 (2008).
32. A. A. Velikanov, *Tr. Inst. Met., Sverdl.*, 18, 143 (1969).
33. A. A. Velikanov and P. P. Shevchuk, *Sov. Electrochem.*, 7, 723 (1971).
34. B. A. Eichis, T. G. Sokolova, and A. A. Velikanov, *Sov. Electrochem.*, 7, 1447 (1971).
35. A. A. Velikanov and B. A. Eichis, *Izv. Vyssh. Uchebn. Zaved., Tsvet. Met.*, 14, 42 (1971).
36. T. Lv, D. Chen, and M. Huang, *J. Appl. Phys.*, 100, 086103 (2006).
37. Akira Egami, Toshio Onoye, and K. Narita, *Trans. Japan Inst. Met.*, 22, 399 (1981).
38. O. V. Andreev and N. N. Parshukov, *Russ. J. Inorg. Chem.*, 36, 1190 (1991).
39. S. O. Engblom, J. C. Myland, and K. B. Oldham, *J. Electroanal. Chem.*, 480, 120 (2000).
40. D. J. Gavaghan and A. M. Bond, *J. Electroanal. Chem.*, 480, 133 (2000).
41. A. M. Bond, N. W. Duffy, S.-X. Guo, J. Zhang, and D. Elton, *Anal. Chem.*, 77, 186A (2005).
42. J. Zhang, S.-X. Guo, and A. M. Bond, *Anal. Chem.*, 79, 2276 (2007).
43. C.-Y. Lee, S.-X. Guo, A. M. Bond, and K. B. Oldham, *J. Electroanal. Chem.*, 615, 1 (2008).
44. M.-E. Wagner, R. Valenzuela, T. Vargas, M. Colet-Lagrange, and A. Allanore, *J. Electrochem. Soc.*, 163, D17 (2016).